Arch. Mech., 49, 3, pp. 547–572, Warszawa 1997

Transformation thermomechanics of R-phase in TiNi shape memory alloys (*)

K. TANAKA, F. NISHIMURA, H. KATO (HINO/TOKYO)
and S. MIYAZAKI (TSUKUBA)

THERMOMECHANICAL BEHAVIOUR in TiNi shape memory alloys after the R-phase transformation is formulated from the continuum mechanical point of view based on two metallurgical processes progressing simultaneously: the lattice distortion in the R-phase and the variants reorientation of the twinned R-phase variants. The start and evolution of both processes are assumed to be governed by conditions similar to the yield condition and the associated consistency condition in plasticity. The evolution equations are derived by solving a conditional extremum problem derived from the dissipation inequality. Uniaxial behaviour is discussed under several thermomechanical load conditions. The simulation of the recovery stress induced during constraint heating presents a clear coupled effect of the two metallurgical processes.

1. Introduction

THE R-PHASE TRANSFORMATION occurs in TiNi shape memory alloys in a certain temperature range just prior to the martensitic transformation [1–4]. The rhombohedral phase is produced from the parent B2 phase during the transformation. The stress-strain curve changes its form from apparent plasticity to pseudoelasticity depending on the test temperature; the former is the shape memory effect exhibiting the recoverable deformation, whereas in the latter, the stress-induced pseudoelasticity is associated with the stress-induced forward and reverse transformations. In almost all cases, the pseudoelasticity is observed in a relatively narrow temperature range without showing any large hysteresis. This is the reason why the R-phase transformation is preferably used in shape memory devices requiring a sensitive response to the input.

Metallurgy tells us that the R-phase transformation starts during thermomechanical loading when a transformation start condition is satisfied, and finishes when a transformation finish condition is fulfilled, forming the twin-related R-phase variants. The twinned structure is self-accommodated under the stress-free state and is preferred by the applied stress, as in the case of the martensitic transformation. The lattice distortion in the R-phase and/or the variants reorientation of the twinned variants then follow in the subsequent thermomechanical loading. The transformation start/finish condition was determined on

(*) Part of the paper has been reported at the 31st Polish Solid Mechanics Conference: SolMec 96 (Mierki, July 10–14, 1996).

the stress-temperature plane, both in the R-phase forward and reverse transformations. The shift and change in the stress-strain or strain-temperature hysteresis loop have rarely been observed during cyclic mechanical or thermal loading because the strain induced by the R-phase transformation is small, less than one tenth of that induced by the martensitic transformation.

Investigations should be carried out from the continuum mechanical point of view to predict as rigorously as possible the elongation and force induced in the shape memory devices during the actual operations. In fact a few studies have been carried out according to the models of R-phase transformation. So far the models employed are all taken from the study of martensitic transformations, meaning that the volume fraction of the R-phase is regarded as an internal variable to measure the extent of R-phase transformation, and the transformation kinetics is characterized as an evolution equation [5–8]. It should, however, be clearly noted that the case is true only during the R-phase transformation. When the thermomechanical load path crosses the R-phase transformation finish line in the stress-temperature space, the strain observed in the subsequent loading is attributed to the temperature-dependence of the lattice constants of the R-phase; in other words, to the lattice distortion in the R-phase and the variants reorientation of the R-phase twinned variants formed in the progress of the preceding R-phase transformation [2, 3]. MIYAZAKI *et al.* [4] measured in the sputter-deposited Ti-Ni thin films that, in the cooling process under constant applied stress, about two times larger amount of strain is further induced after the R-phase transformation, and proved that the strain is due both to the lattice distortion in the R-phase and the variants reorientation of the twinned R-phase variants. The growth of the strain is misunderstood in the Refs. [5–8] to be the response in the R-phase transformation. Theoretical descriptions carried out so far on the thermomechanical behaviour of the R-phase are, therefore (although some qualitative/quantitative coincidence is observed between the prediction and the experimental observations), not acceptable. A new theoretical framework should be established fully based on the results of metallurgical study.

In this paper, the thermomechanical behaviour of the R-phase in TiNi shape memory alloys is discussed from the macroscopic point of view, not during the R-phase transformation but after it, in order to emphasize that the alloy response after the R-phase transformation plays an important role in the design of the shape memory alloy devices. The two types of the microscopic structural changes, the lattice distortion in the R-phase and the variants reorientation of the twinned R-phase variants, are regarded to be responsible for the macroscopic thermomechanical behaviour of the alloys. A unified macroscopic theory is constructed by solving a conditional extremum problem subject to the conditions of these microscopic fundamental processes. Constitutive equations, thermomechanical and calorimetric, are derived together with the evolution equations for the lattice distortion in the R-phase and the variants reorientation. The uniaxial case is discussed numerically referring to the experimental observations.

2. Metallurgy in R-phase transformation and subsequent thermomechanical process

The metallurgical study [1–3, 9, 10] has clearly revealed that the unit cell of the R-phase is created from the parent B2 cell by elongating the lattice along any one of the <111> directions, as shown in Fig. 1 a. The length of the three axes remains unchanged during this R-phase transformation while the rhombohedral angle α (cf. Fig. 1 b) changes. Upon cooling under constant applied stress, the nucleation of the R-phase starts at a critical temperature which strongly depends on the applied stress. In a narrow temperature region, of the order of less than 10 K, the R-phase transformation progresses, inducing the transformation strain. The rhombohedral angle α decreases sharply.

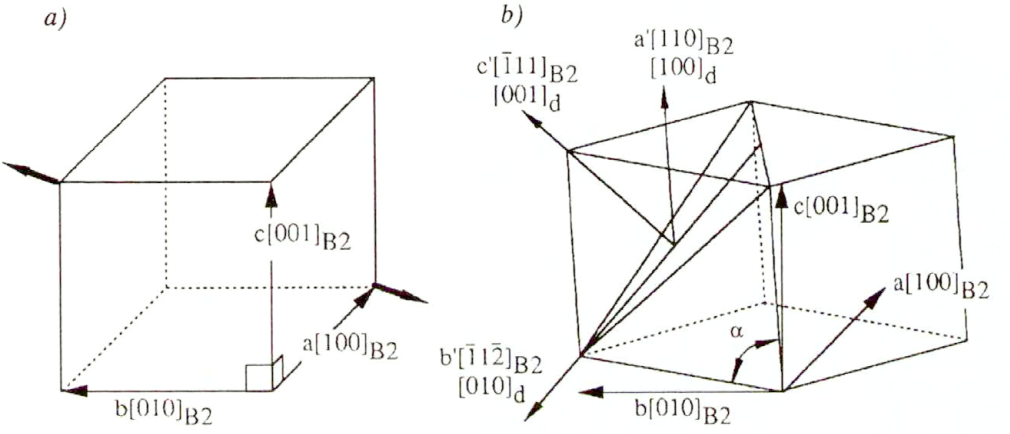

FIG. 1. R-phase transformation in unit cell.

Then the lattice distortion follows in the R-phase. Its extent can be measured by means of the rhombohedral angle α, which depends solely on the temperature T in the TiNi alloy [3, 4, 11, 12];

$$\alpha = \alpha(T). \tag{2.1}$$

Some macroscopic deformation may also be induced due directly to the change in α. The main source of the macroscopic deformation is, however, the variants reorientation occurring in the self-accommodated twinned variants through the migration of the twin boundaries [2]. In the coalescence process, the thermally-induced R-phase variants convert to the stress-preferred variants by twinning deformation process, leading finally to a single variant crystal. This variants reorientation process results in a macroscopic deformation till the value of the strain reaches a maximum recoverable strain which has been "stored" in the alloy during the self-accommodation process [2].

The R-phase formed in the alloy during cooling transforms back to the original parent phase in the subsequent heating process just after the lattice constants

of the R-phase become close to those of the parent B2 phase. The reverse transformation takes place by being associated with a very small strain change as the first-order transformation [13], as in the case of the forward transformation, at the reverse transformation temperature which also depends on the applied stress. Thus, the R-phase transformation has a hysteresis although it is very small corresponding to the small strain change, meaning that Eq. (2.1) has different functional forms on cooling and heating, respectively. However, again the major part of the recovery strain upon heating appears as a function of temperature in the second-order transformation manner until the reverse transformation takes place in the first-order transformation manner.

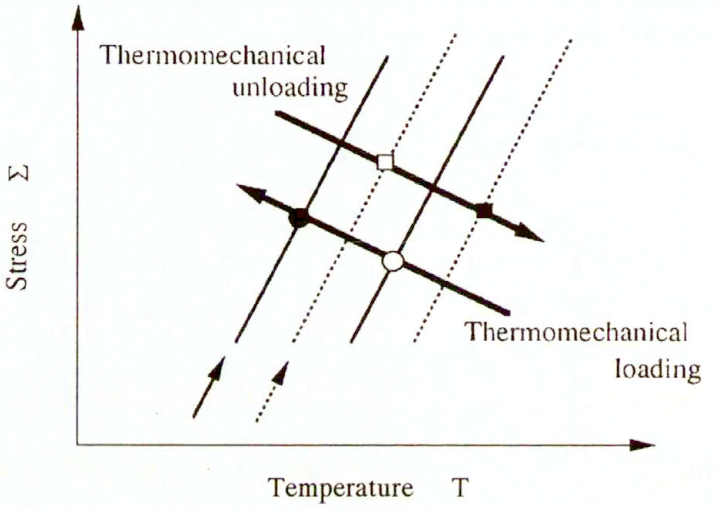

FIG. 2. R-phase forward and reverse transformation lines (schematic).

Explaining the situation in the stress (Σ) – temperature (T) plane in Fig. 2, the R-phase transformation starts when the thermomechanical loading path meets the transformation start line at the hollow circle in the figure, and finishes on the transformation finish line at the solid circle. The R-phase transformation zone bounded by the transformation start/finish (solid) lines is narrow. The lattice distortion and the variants reorientation processes go on in the R-phase in the subsequent thermomechanical loading. During thermomechanical unloading, the R-phase reverse transformation starts on the R-phase reverse transformation line at the hollow box in the figure, and finishes on the R-phase reverse transformation line at the solid box. The R-phase reverse transformation zone, bounded by the reverse transformation start/finish (broken) lines, is also narrow. The present discussion takes notice of the alloy behaviour when the load state (Σ, T) is on the left side of either the R-phase finish line (solid arrow) in the loading process or the R-phase reverse transformation start line (broken arrow) in the unloading process. The width of these two lines was measured to be very narrow, less

than 5 K, corresponding to the small strain change associated with the R-phase transformation. The lines are called in the following discussion the R-phase transformation line and the R-phase reverse transformation line, respectively.

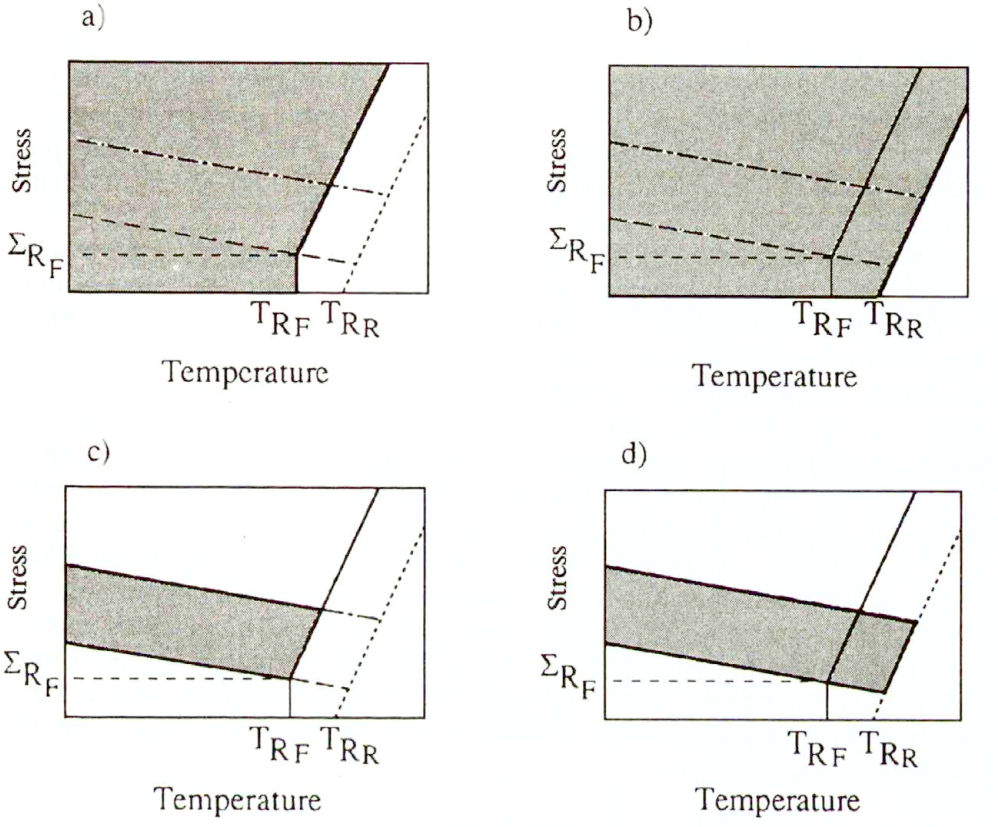

FIG. 3. Transformation lines (schematic).

A series of extensive experimental study on the R-phase transformation in TiNi shape memory alloys [1–4] has revealed the conditions of the lattice distortion in the R-phase and of the variants reorientation of the R-phase variants to undergo the uniaxial thermomechanical loading. The results are summarized schematically in Fig. 3 on the applied stress-temperature plane (see BARRETT [14] and BRINSON *et al.* [15] for similar sketch for the martensitic transformation). The R-phase transformation finishes when the thermomechanical load state (T, Σ) reaches the R-phase transformation line, the thick straight lines starting from the point (T_{R_F}, Σ_{R_F}) in Fig. 3 a. The lattice distortion in the R-phase progresses when the thermomechanical load point is inside the shaded region shown in Fig. 3 a and moves with $\dot{T} < 0$. The upper section of the R-phase transformation line has a very high value in slope c, of nearly $c \approx 10\,\mathrm{MPa/K}$, whereas the lower section is temperature-independent. The reverse lattice distortion, on the other hand,

occurs in the shaded region sketched in Fig. 3 b when the load state moves with $\dot{T} > 0$. Another straight line intersecting the horizontal axis at $(T_{R_R}, 0)$, almost parallel to the upper section of the R-phase transformation line, is the R-phase reverse transformation line at which the reverse transformation starts with an associated small strain recovery. The R-phase reverse transformation line might have a critical stress as in the case of the R-phase transformation line, meaning that the section of the line below the critical stress might be temperature-independent. Since no definite experimental data is available so far with respect to this point, the straight line in Fig. 3 b is employed here as the R-phase reverse transformation line.

The variants reorientation of the R-phase variants progresses by twinning only when the R-phase variants exist in the alloy and the load state is either in the shaded region in Fig. 3 c during cooling or in the shaded region in Fig. 3 d during heating. The variants reorientation start line, the lower boundary of the region, exhibits a clear temperature-dependence since, firstly, the mobility of the twin boundaries becomes lower with the decreasing strain due to twinning, and secondly, the process is essentially a thermal activation process. The temperature-dependence is almost linear. The process completes on the variants reorientation finish line, the upper boundary of the region, which is almost parallel to the start line. A preferred variant is formed inside the alloy depending on the applied stress. A comment: there exists no definite experimental proof which shows that the variants reorientation start line intersects with the R-phase transformation line at the point (T_{R_F}, Σ_{R_F}). The point of intersection is in fact expected to be below, but not far from, the point. In this study the situation illustrated in Fig. 3 c is assumed for simplicity with the understanding that the sketch must be not very far from the actual situation.

3. State variables during lattice distortion and variants reorientation

Let us consider the thermomechanical behaviour in a shape memory alloy which, after having finished the R-phase transformation, is in the process of both the lattice distortion in the R-phase and the crystal reorientation under thermal and/or mechanical loading.

The extent of the lattice distortion in the R-phase can, as explained in the preceding section, be described in an appropriate representative volume of the alloy by means of a value α of the rhombohedral angle defined in Eq. (2.1) [4]. A twinned structure is produced in the variants as a result of the R-phase transformation. In most cases the deformation associated with the R-phase transformation is averaged to be null from the macroscopic point of view since the self-accommodation process goes on during the R-phase transformation. The internal twinned structure is formed during the process so that a certain amount of strain, the recoverable strain, is induced in the subsequent variants reorientation

process. In this study, the self-accommodation is understood to be a phenomenon in which the possibility to produce a certain amount of recoverable strain, $\boldsymbol{\Omega}^*$, say, is stored in the variants. The strain is induced as a macroscopic deformation during the subsequent thermomechanical loading. Under the presence of load, however, the self-accommodation is not realized but a different crystallographic structure is attained depending on the stress state to minimize the free energy of the alloy. The same amount of recoverable strain is, nevertheless, "stored" in the alloy to be induced macroscopically in the subsequent thermomechanical processes. The recoverable strain $\boldsymbol{\Omega}^*$ is assumed to be simply governed by the equation

$$\dot{\boldsymbol{\Omega}}^* = \boldsymbol{\Omega}^*_\alpha \dot{\alpha}, \tag{3.1}$$

where the material coefficient tensor $\boldsymbol{\Omega}^*_\alpha$ is determined by means of the thermomechanical state at the instant of R-phase transformation.

Upon loading, the twinned structure in the alloy changes through the variants reorientation, inducing a macroscopic deformation [2]. The extent of the process on the microscopic structural level can be characterized by a set of scalar variables which represent the volume fractions of the pairs of martensite twin and of one variant comprising a twin pair [16–19].

By averaging these variables over a representative volume in the alloy, one can introduce the macroscopic variables $(\zeta_1, \zeta_2, \ldots)$, say, which represent the microscopic alloy structure. The evolution equations of these internal variables estimate the change in the microscopic alloy structure.

In the present study, for the sake of simplicity, two internal variables (α, ζ) are chosen to characterize the lattice distortion in the R-phase and the variants reorientation processes, leaving a generalization of the theory for the next study. LECLERCQ and LEXCELLENT [19] have developed a generalized theory of shape memory alloys by introducing the volume fractions of the thermal-induced martensite and of the oriented martensite variants which corresponds to the present ζ, and suggested that the theory could be applied to transformation thermomechanics of the R-phase, too. It can be applied if the lattice distortion is taken into account in addition.

It should be noted that hereafter, for the sake of theoretical convenience, the internal variable α is understood to be the angle $\pi/2 - \alpha$ with the rhombohedral angle α illustrated in Fig. 1 b. It takes, therefore, a value in $[0, (\pi/2))$, whereas the variable ζ is normalized to have a value in [0,1].

When the lattice distortion and/or the crystal reorientation take place, a macroscopic irreversible strain tensor $\mathbf{E}^*$ is induced, which is also employed here as another internal variable.

Let us propose that the Green strain tensor $\mathbf{E}$ can be additively decomposed in the rate form,

$$\dot{\mathbf{E}} = \dot{\mathbf{E}}^e + \dot{\mathbf{E}}^*, \tag{3.2}$$

where $\dot{\mathbf{E}}^e$ stands for the elastic component while $\dot{\mathbf{E}}^*$ is the irreversible component due to the lattice distortion in the R-phase and the variants reorientation [19]. For the irreversible strain $\mathbf{E}^*$, the following kinematical relation is assumed:

$$\dot{\mathbf{E}}^* = \mathbf{E}^*_\alpha(\alpha, \zeta; \boldsymbol{\Sigma}, T)\dot{\alpha} + \boldsymbol{\Omega}^*\dot{\zeta}\,, \tag{3.3}$$

representing an additive decomposition into the terms due to the lattice distortion in the R-phase and to the variants reorientation, where $\boldsymbol{\Sigma}$ and T denote the stress tensor and the temperature, respectively. The second term on the right-hand side clearly states that, assuming $\boldsymbol{\Omega}^*$ be constant during the process, $\boldsymbol{\Omega}^*$ can be read as the macroscopic strain at the completion of the variants reorientation process. This is the reason why $\boldsymbol{\Omega}^*$ is called the recoverable strain. The first term covers the case in which the lattice distortion process might directly produce a macroscopic deformation, very likely under the stressed state.

4. Unified thermomechanical theory of lattice distortion in R-phase and variants reorientation

In order to construct a unified theory of the lattice distortion in the R-phase and variants reorientation in shape memory alloys, let us start from the energy balance and the Clausius–Duhem inequality [20, 21];

$$\varrho\dot{U} - \boldsymbol{\sigma} : \mathbf{L} + \operatorname{div}\mathbf{q} - \varrho\sigma = 0, \qquad \varrho\dot{\eta} - \frac{\sigma}{T} + \operatorname{div}\left(\frac{\mathbf{q}}{T}\right) \geq 0, \tag{4.1}$$

where, here and henceforth, the variables have the following physical significance: ϱ, ϱ_0 – densities in the current and reference configurations, respectively, U – internal energy density, $\boldsymbol{\sigma}$ – Cauchy stress tensor, $\mathbf{L} = \dot{\mathbf{F}}\cdot\dot{\mathbf{F}}^{-1}$ – velocity gradient with $\mathbf{F}$ being the deformation gradient, $\mathbf{q}$ – heat flux, σ – heat production term, η – entropy density.

Throughout this study the notation div stands for the divergence with respect to the Eulerian coordinate, while Grad is the gradient with respect to the Lagrangean coordinate, respectively.

Following standard continuum thermodynamics, one can reach the relations

$$\begin{aligned} &\mathbf{E}^e = -\varrho_0\frac{\partial\Psi}{\partial\boldsymbol{\Sigma}}, \qquad \eta = -\frac{\partial\Psi}{\partial T}, \\ &\mathcal{D} = K_1\dot{\alpha} + K_2\dot{\zeta} - \frac{1}{T}\mathbf{Q}\cdot\operatorname{Grad}T \geq 0, \end{aligned} \tag{4.2}$$

where

$$\Psi = \Psi(\boldsymbol{\Sigma}, T; \alpha, \zeta, \mathbf{E}^*) = U - \eta T - \frac{1}{\varrho_0}\boldsymbol{\Sigma} : \mathbf{E}^e \tag{4.3}$$

represents the Gibbs free energy, and the second Piola – Kirchhoff stress tensor $\boldsymbol{\Sigma}$, the material heat flux $\mathbf{Q}$ and the thermodynamic forces K_1 and K_2 are defined by

$$\boldsymbol{\Sigma} = \frac{\varrho_0}{\varrho}\mathbf{F}^{-1}\cdot\boldsymbol{\sigma}\cdot\mathbf{F}^{-T}, \qquad \mathbf{Q} = \frac{\varrho_0}{\varrho}\mathbf{F}^{-1}\cdot\mathbf{q},$$

$$K_1 = -\varrho_0\frac{\partial\Psi}{\partial\alpha} + \left(\boldsymbol{\Sigma} - \varrho_0\frac{\partial\Psi}{\partial\mathbf{E}^*}\right) : \mathbf{E}^*_\alpha, \tag{4.4}$$

$$K_2 = -\varrho_0\frac{\partial\Psi}{\partial\zeta} + \left(\boldsymbol{\Sigma} - \varrho_0\frac{\partial\Psi}{\partial\mathbf{E}^*}\right) : \boldsymbol{\Omega}^*.$$

Equations $(4.2)_{1,2}$ govern the reversible thermomechanical process of the material, from which one can derive the thermomechanical and calorimetric constitutive equations in rate form if the elastic process is reasonably assumed to be not influenced by the irreversible processes [20, 22]:

$$\dot{\mathbf{E}}^e = \mathbf{S} : \dot{\boldsymbol{\Sigma}} + \boldsymbol{\Theta}\dot{T}, \qquad \dot{\eta} = \frac{\boldsymbol{\Theta}}{\varrho_0} : \dot{\boldsymbol{\Sigma}} + Tc\dot{T},$$

$$\mathbf{S} = -\varrho_0\frac{\partial^2\Psi}{\partial\boldsymbol{\Sigma}\partial\boldsymbol{\Sigma}}, \qquad \boldsymbol{\Theta} = -\varrho_0\frac{\partial^2\Psi}{\partial\boldsymbol{\Sigma}\partial T}, \qquad c = -\frac{\varrho_0}{T}\frac{\partial^2\Psi}{\partial T^2}, \tag{4.5}$$

where $\mathbf{S}$ stands for the elastic compliance tensor while $\boldsymbol{\Theta}$ and c correspond to the thermoelastic tensor and the specific heat, respectively.

Later consideration is limited to the case of the processes in which the following dissipation inequality holds:

$$\mathcal{D} = K_1\dot{\alpha} + K_2\dot{\zeta} \geq 0, \tag{4.6}$$

and the thermomechanical constitutive equation is solely discussed.

5. Evolution equations in irreversible processes

The thermomechanical study on the R-phase transformation carried out so far in metallurgy [1 – 3] allows one to assume that, as in plasticity with the yield condition, the lattice distortion in the R-phase occurs only under a thermomechanical restriction

$$f = f(\boldsymbol{\Sigma}, T; K_1, K_2; \alpha, \zeta) = 0 \qquad \text{and} \qquad \dot{f} = 0. \tag{5.1}$$

Figures 3 a and b actually provide a uniaxial picture of this condition in TiNi shape memory alloy. It is worthwhile to note that the time t is included in Eq. (5.1) as an implicit parameter through the state variables, which reflects the fact that the lattice distortion process is diffusionless.

The variants reorientation is activated under the condition that a twinned structure has already been formed in the alloy, being independent of whether the

lattice distortion in the R-phase progresses or not, and produces a corresponding macroscopic deformation [2, 3]. It is natural to assume that the process is governed by a thermomechanical condition

$$g = g(\boldsymbol{\Sigma}, T; K_1, K_2; \alpha, \zeta) = 0 \qquad \text{and} \qquad \dot{g} = 0, \tag{5.2}$$

which is a mathematical rephrase of the actual situation illustrated in Figs. 3c, d.

The transformation start condition and the associated consistency condition during the process of transformation have been discussed in the Refs. [17–19, 21] in the case of martensitic transformations. PATOOR *et al.* [18] have pointed out, from the micromechanical point of view, that the transformation condition should include the third invariant of the deviatoric stress tensor as one of the variables, in addition to the von Mises-type second variant of the deviatoric stress tensor. The shift of the transformation lines, which represents the consistency conditions, have experimentally been investigated in an Fe-based shape memory alloy [23, 24].

The requirement of the second law of thermodynamics (4.6) can be re-read as a conditional extremum problem of

$$\overline{\mathcal{D}} = \mathcal{D} - \dot{\lambda} f - \dot{\mu} g = K_1 \dot{\alpha} + K_2 \dot{\zeta} - \dot{\lambda} f - \dot{\mu} g \tag{5.3}$$

with the Lagrange multipliers $\dot{\lambda}$ and $\dot{\mu}$ [25–27]. The usual procedure yields the final formulae

$$\dot{\alpha} = \dot{\lambda} \frac{\partial f}{\partial K_1} + \dot{\mu} \frac{\partial g}{\partial K_1}, \qquad \dot{\zeta} = \dot{\lambda} \frac{\partial f}{\partial K_2} + \dot{\mu} \frac{\partial g}{\partial K_2}, \tag{5.4}$$

which represent the evolution equations for the internal variables α and ζ.

For the sake of compact presentation of the theory, the generalized thermodynamic force $\mathbf{K} = (K_1, K_2)$ is introduced, and an appropriate inner product $*$ is defined for the quantities relating to $\mathbf{K}$, i.e., for example,

$$\frac{\partial f}{\partial \mathbf{K}} * \frac{\partial \mathbf{K}}{\partial \alpha} = \frac{\partial f}{\partial K_1} \frac{\partial K_1}{\partial \alpha} + \frac{\partial f}{\partial K_2} \frac{\partial K_2}{\partial \alpha}.$$

The Lagrange multipliers introduced in Eq. (5.3) can be determined from the consistency conditions, Eqs. $(5.1)_2$ and $(5.2)_2$:

$$\begin{aligned}
\dot{f} &= \left(\frac{\partial f}{\partial \boldsymbol{\Sigma}} + \frac{\partial f}{\partial \mathbf{K}} * \frac{\partial \mathbf{K}}{\partial \boldsymbol{\Sigma}} \right) : \dot{\boldsymbol{\Sigma}} + \left(\frac{\partial f}{\partial T} + \frac{\partial f}{\partial \mathbf{K}} * \frac{\partial \mathbf{K}}{\partial T} \right) \dot{T} \\
&\quad + \left(\frac{\partial f}{\partial \alpha} + \frac{\partial f}{\partial \mathbf{K}} * \frac{\partial \mathbf{K}}{\partial \alpha} \right) \dot{\alpha} + \left(\frac{\partial f}{\partial \zeta} + \frac{\partial f}{\partial \mathbf{K}} * \frac{\partial \mathbf{K}}{\partial \zeta} \right) \dot{\zeta} = 0, \\
\dot{g} &= \left(\frac{\partial g}{\partial \boldsymbol{\Sigma}} + \frac{\partial g}{\partial \mathbf{K}} * \frac{\partial \mathbf{K}}{\partial \boldsymbol{\Sigma}} \right) : \dot{\boldsymbol{\Sigma}} + \left(\frac{\partial g}{\partial T} + \frac{\partial g}{\partial \mathbf{K}} * \frac{\partial \mathbf{K}}{\partial T} \right) \dot{T} \\
&\quad + \left(\frac{\partial g}{\partial \alpha} + \frac{\partial g}{\partial \mathbf{K}} * \frac{\partial \mathbf{K}}{\partial \alpha} \right) \dot{\alpha} + \left(\frac{\partial g}{\partial \zeta} + \frac{\partial g}{\partial \mathbf{K}} * \frac{\partial \mathbf{K}}{\partial \zeta} \right) \dot{\zeta} = 0.
\end{aligned} \tag{5.5}$$

The result reads as

$$
\begin{aligned}
\dot{\lambda} &= \overline{\Delta}\left(-\frac{\partial g}{\partial K_1}\mathbf{Z}_{\Sigma} + \frac{\partial g}{\partial K_2}\mathbf{A}_{\Sigma}\right) : \dot{\boldsymbol{\Sigma}} + \overline{\Delta}\left(-\frac{\partial g}{\partial K_1}Z_T + \frac{\partial g}{\partial K_2}A_T\right)\dot{T}, \\
\dot{\mu} &= \overline{\Delta}\left(\frac{\partial f}{\partial K_1}\mathbf{Z}_{\Sigma} - \frac{\partial f}{\partial K_2}\mathbf{A}_{\Sigma}\right) : \dot{\boldsymbol{\Sigma}} + \overline{\Delta}\left(\frac{\partial f}{\partial K_1}Z_T - \frac{\partial f}{\partial K_2}A_T\right)\dot{T}, \\
\mathbf{A}_{\Sigma} &= \Delta\left(-g_{\zeta}f_{\Sigma} + f_{\zeta}g_{\Sigma}\right), \qquad A_T = \Delta\left(-g_{\zeta}f_T + f_{\zeta}g_T\right), \\
\mathbf{Z}_{\Sigma} &= \Delta\left(g_{\alpha}f_{\Sigma} - f_{\alpha}g_{\Sigma}\right), \qquad Z_T = \Delta\left(g_{\alpha}f_T - f_{\alpha}g_T\right), \\
f_{\Sigma} &= \frac{\partial f}{\partial \mathbf{K}} * \frac{\partial \mathbf{K}}{\partial \boldsymbol{\Sigma}} + \frac{\partial f}{\partial \boldsymbol{\Sigma}}, \qquad f_T = \frac{\partial f}{\partial T} + \frac{\partial f}{\partial \mathbf{K}} * \frac{\partial \mathbf{K}}{\partial T}, \\
g_{\Sigma} &= \frac{\partial g}{\partial \boldsymbol{\Sigma}} + \frac{\partial g}{\partial \mathbf{K}} * \frac{\partial \mathbf{K}}{\partial \boldsymbol{\Sigma}}, \qquad g_T = \frac{\partial g}{\partial T} + \frac{\partial g}{\partial \mathbf{K}} * \frac{\partial \mathbf{K}}{\partial T}, \\
f_{\alpha} &= \frac{\partial f}{\partial \mathbf{K}} * \frac{\partial \mathbf{K}}{\partial \alpha} + \frac{\partial f}{\partial \alpha}, \qquad f_{\zeta} = \frac{\partial f}{\partial \mathbf{K}} * \frac{\partial \mathbf{K}}{\partial \zeta} + \frac{\partial f}{\partial \zeta}, \\
g_{\alpha} &= \frac{\partial g}{\partial \mathbf{K}} * \frac{\partial \mathbf{K}}{\partial \alpha} + \frac{\partial g}{\partial \alpha}, \qquad g_{\zeta} = \frac{\partial g}{\partial \mathbf{K}} * \frac{\partial \mathbf{K}}{\partial \zeta} + \frac{\partial g}{\partial \zeta}, \\
\Delta^{-1} &= f_{\alpha}g_{\zeta} - f_{\zeta}g_{\alpha}, \qquad \overline{\Delta}^{-1} = \frac{\partial f}{\partial K_1}\frac{\partial g}{\partial K_2} - \frac{\partial f}{\partial K_2}\frac{\partial g}{\partial K_1},
\end{aligned}
\tag{5.6}
$$

and the evolution equations of the internal variables α and ζ are given by

$$
\dot{\alpha} = \mathbf{A}_{\Sigma} : \dot{\boldsymbol{\Sigma}} + A_T\dot{T}, \qquad \dot{\zeta} = \mathbf{Z}_{\Sigma} : \dot{\boldsymbol{\Sigma}} + Z_T\dot{T}. \tag{5.7}
$$

Equation $(5.7)_1$ governs the progress of the lattice distortion in the R-phase, whereas Eq. $(5.7)_2$ – the progress of variants reorientation. Equation (5.7) state that both processes are rate-independent, or diffusionless according to the terminology in metallurgy.

The irreversible strain rate $\dot{\mathbf{E}}^*$ due to the lattice distortion and the variants reorientation can be obtained from Eqs. (5.7) and (3.4) to be

$$
\dot{\mathbf{E}}^* = \left(\mathbf{E}^*_{\alpha} \otimes \mathbf{A}_{\Sigma} + \boldsymbol{\Omega}^* \otimes \mathbf{Z}_{\Sigma}\right) : \dot{\boldsymbol{\Sigma}} + \left(\mathbf{E}^*_{\alpha}A_T + \boldsymbol{\Omega}^*Z_T\right)\dot{T}, \tag{5.8}
$$

which, together with Eqs. (3.2) and $(4.5)_1$, finally leads to the following thermomechanical constitutive equation in rate form:

$$
\dot{\mathbf{E}} = \left(\mathbf{S} + \mathbf{E}^*_{\alpha} \otimes \mathbf{A}_{\Sigma} + \boldsymbol{\Omega}^* \otimes \mathbf{Z}_{\Sigma}\right) : \dot{\boldsymbol{\Sigma}} + \left(\boldsymbol{\Theta} + \mathbf{E}^*_{\alpha}A_T + \boldsymbol{\Omega}^*Z_T\right)\dot{T}. \tag{5.9}
$$

The dissipation inequality (4.6) delivers

$$
\mathcal{D} = \dot{\lambda}\left(\mathbf{K} * \frac{\partial f}{\partial \mathbf{K}}\right) + \dot{\mu}\left(\mathbf{K} * \frac{\partial g}{\partial \mathbf{K}}\right) \geq 0, \tag{5.10}
$$

which states that the lattice distortion in the R-phase and the variants reorientation progress when

$$\dot{\lambda} > 0 \qquad \text{and} \qquad \dot{\mu} > 0 \tag{5.11}$$

hold, respectively, under the situation in which the conditions

$$\mathbf{K} * \frac{\partial f}{\partial \mathbf{K}} \geq 0, \qquad \mathbf{K} * \frac{\partial g}{\partial \mathbf{K}} \geq 0 \tag{5.12}$$

always hold. The condition (5.11) can be used, like the loading condition in conventional plasticity, to judge whether the process starts, continues or stops during an applied thermomechanical loading $(\dot{T}, \dot{\boldsymbol{\Sigma}})$.

6. Analysis of uniaxial behaviour

6.1. Fundamental uniaxial relations

Although the experimental results shown in Fig. 3 could be summarized to give an explicit form of the functions f and g introduced in Eqs. (5.1) and (5.2), here in this study the uniaxial analysis on the behaviour in TiNi shape memory alloy is carried out starting directly from Fig. 3, leaving the construction of a fully closed description of the phenomena to the next study. The uniaxial version of the relations developed so far and the additional assumptions are as follows: The progress of the lattice distortion in the R-phase is independent of the applied stress Σ and is governed by

$$\dot{\alpha} = A_T \dot{T} \qquad \text{with} \qquad A_T = a_c(A_{T0} - \alpha), \tag{6.1}$$

where a_c and A_{T0} are the constant material parameters. The evolution equation (6.1) is solved to give a direct form

$$\alpha = A_{T0}\left[1 - \exp a_c(T^*_{R_F} - T)\right], \tag{6.2}$$

where $T^*_{R_F}$ is the temperature on the R-phase transformation start line (see the experimental observation by MIYAZAKI *et al.* [4]). When $\Sigma < \Sigma_{R_F}$, $T^*_{R_F} = T_{R_F}$ as is seen in Fig. 3 a.

The variants reorientation, characterized uniaxially by

$$\dot{\zeta} = Z_\Sigma \dot{\Sigma} + Z_T \dot{T}, \tag{6.3}$$

is assumed, following the experimental observation [3], to have an explicit form

$$\dot{\zeta} = (1 - \zeta)\overline{Z}_\Sigma \left(\dot{\Sigma} + b\dot{T}\right), \tag{6.4}$$

where $b > 0$ and $\overline{Z}_\Sigma$ denote the constant material parameters. Integrating Eq. (6.4) and taking into account the fact that the point (T_{R_F}, Σ_{R_F}) is on the start line ($\zeta = 0$), one has

$$\zeta = 1 - \exp \overline{Z}_\Sigma [b(T_{R_F} - T) + (\Sigma_{R_F} - \Sigma)] . \tag{6.5}$$

The variants reorientation start line in Fig. 3c is given by inserting $\zeta = 0$ into Eq. (6.6) as

$$\Sigma = \Sigma_{R_F} - b(T - T_{R_F}), \tag{6.6}$$

which reveals that $-b$ stands for the slope of the variants reorientation start line in the $\Sigma - T$ plane. On the contrary, if $\zeta = 0.99$ is assumed to be the completion of the variants reorientation, the variants reorientation finish line is expressed by

$$\Sigma = \Sigma_{R_F} - b(T - T_{R_F}) + (\ln 100)/\overline{Z}_\Sigma . \tag{6.7}$$

The iso-ζ lines are parallel to the variants reorientation start/finish lines, and to each other.

In order that ζ can move in the interval $[0, 1]$ when the thermomechanical load is in the shaded region in Fig. 3c, the conditions

$$(\ln 100)/\overline{Z}_\Sigma \geq \Sigma - \Sigma_{R_F} + b(T - T_{R_F}) \geq 0 \qquad \text{and} \qquad \overline{Z}_\Sigma > 0, \tag{6.8}$$

must be satisfied. The forward process, $\dot{\zeta} > 0$, occurs only when

$$\dot{\Sigma} + b\dot{T} > 0 \tag{6.9}$$

holds. The relation well explains the experimental observation that no variants reorientation progresses in the isostatic cooling processes ($\dot{\Sigma} = 0$ and $\dot{T} < 0$).

The recoverable strain Ω^* in the variants is assumed to be formed during the lattice distortion process according to

$$\dot{\Omega}^* = \Omega^*_\alpha \dot{\alpha} , \tag{6.10}$$

where Ω^*_α is a constant material parameter. Equation (6.10) states, therefore, nothing other than a linear relation

$$\Omega^* = \Omega^*_\alpha \alpha . \tag{6.11}$$

The uniaxial macroscopic strain due both to the lattice distortion in the R-phase and the crystal reorientation is given by

$$\dot{E}^* = E^*_\alpha \dot{\alpha} + \Omega^* \dot{\zeta} , \tag{6.12}$$

where the material parameter E_α^* is proposed to be expressed as

$$E_\alpha^* = E_{\alpha 0}^* \zeta_s^* \tag{6.13}$$

with a constant material parameter $E_{\alpha 0}^*$, and ζ_s^* denotes the value of the extent of variants reorientation at the point where the thermomechanical loading path crosses the R-phase transformation line. The final expression for $\dot{E}^*$ in Eq. (6.12) is now given by

$$\dot{E}^* = E_{\alpha 0}^* \zeta_s^* \dot{\alpha} + \Omega_\alpha^* \alpha \dot{\zeta}\,. \tag{6.14}$$

It should be noted that $\dot{\alpha}$ and $\dot{\zeta}$ in Eq. (6.14) are linearly connected to $\dot{\Sigma}$ and $\dot{T}$ as can be understood from Eqs. (6.1) and (6.4). So is $\dot{E}^*$, too.

The uniaxial constitutive equation is now obtained from Eqs. (3.3), $(4.5)_1$ and (6.14) in rate form as

$$\dot{E} = S\dot{\Sigma} + \Theta \dot{T} + \dot{E}^*. \tag{6.15}$$

6.2. Cooling under free stress followed by isothermal loading

On the first cooling run down to T_t under $\Sigma = 0$, the lattice distortion in the R-phase starts at T_{R_F} in Fig. 3 a. The angle α has a value determined from Eq. (6.3) at T_t, and the recovery strain "stored" in the alloy is estimated by

$$\Omega^* = \Omega_\alpha^* \alpha = \Omega_\alpha^* A_{T0} \left[1 - \exp a_c (T_{R_F}^* - T_t)\right]. \tag{6.16}$$

Since no variants reorientation progresses during this constant stress loading below Σ_{R_F} (cf. Fig. 3 c), it means, since $\zeta_s^* = 0$, that no macroscopic strain is induced in the process;

$$E_{\text{isostatic}}^* = 0. \tag{6.17}$$

In the subsequent isothermal loading the variants reorientation progresses from the start line on. The strain can, therefore, be calculated by means of Eqs. (6.5), (6.12) and (6.16) as

$$E^* = \int_0^\zeta \Omega_\alpha^* \alpha \, d\zeta = \Omega_\alpha^* \alpha \int_{\Sigma_{ts}}^{\Sigma} \overline{Z}_\Sigma \exp \overline{Z}_\Sigma \left[b(T_{R_F} - T_t) + (\Sigma_{R_F} - \Sigma)\right] d\Sigma, \tag{6.18}$$

where in the first equation the upper limit ζ is given by Eq. (6.5) with $T = T_t$, whereas in the second equation Σ_{ts} denotes the variants reorientation start stress at T_t; i.e.,

$$\Sigma_{ts} = \Sigma_{R_F} - b(T_t - T_{R_F}). \tag{6.19}$$

When the specimen is loaded up to a stress value higher than the variants reorientation finish line (cf. Fig. 3 c), the macroscopic strain observed after the second isothermal run reads from Eq. (6.18) as

$$E^*_{\text{isothermal}} = \Omega^*_\alpha \alpha \,. \tag{6.20}$$

The total strain observed after the whole process is, therefore, estimated by

$$E^*_{\max} = E^*_{\text{isostatic}} + E^*_{\text{isothermal}} = \Omega^*_\alpha A_{T0}[1 - \exp a_c(T_{R_F} - T)] \,, \tag{6.21}$$

which is measured as the residual strain after the full elastic unloading. The temperature-dependence of $E^*_{\max}$ given in Eq. (6.21) (cf. Fig. 4) explains well the experimental observations [2].

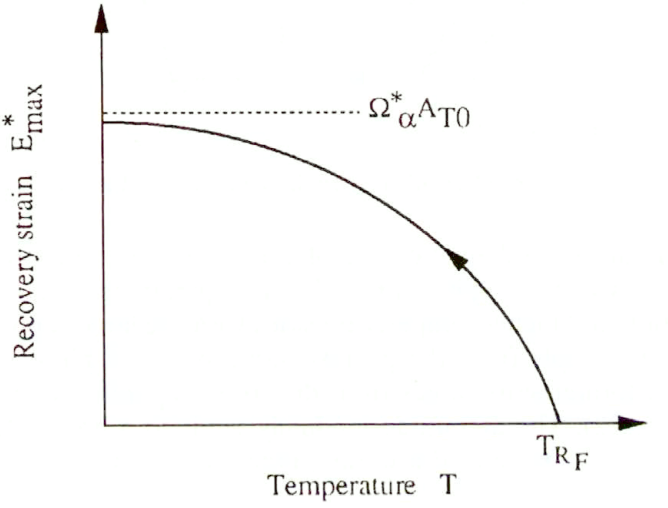

FIG. 4. Temperature dependence of recovery strain (schematic).

6.3. Cooling under constant applied stress

The isostatic cooling under a constant applied stress Σ^* does, as explained above in relation to Eq. (6.17), not drive the variants reorientation in the thermally-induced R-phase twinned structure. The macroscopic strain observed at the end of the cooling down to T is, therefore, calculated from Eq. (6.14) by

$$\begin{aligned} E^* &= E^*_{\alpha 0} \zeta^*_s \alpha \\ &= E^*_{\alpha 0} A_{T0} \left[1 - \exp \overline{Z}_\Sigma \left(\frac{b}{c} - 1\right)(\Sigma^* - \Sigma_{R_F})\right] \left[1 - \exp a_c \left(T^*_{R_F} - T\right)\right] , \end{aligned} \tag{6.22}$$

when the upper section of the R-phase transformation line is expressed by

$$\Sigma = \Sigma_{R_F} + c(T - T_{R_F}) \tag{6.23}$$

with the slope $c > 0$ of the line, therefore, when

$$T^*_{R_F} = T_{R_F} + (\Sigma^* - \Sigma_{R_F})/c. \tag{6.24}$$

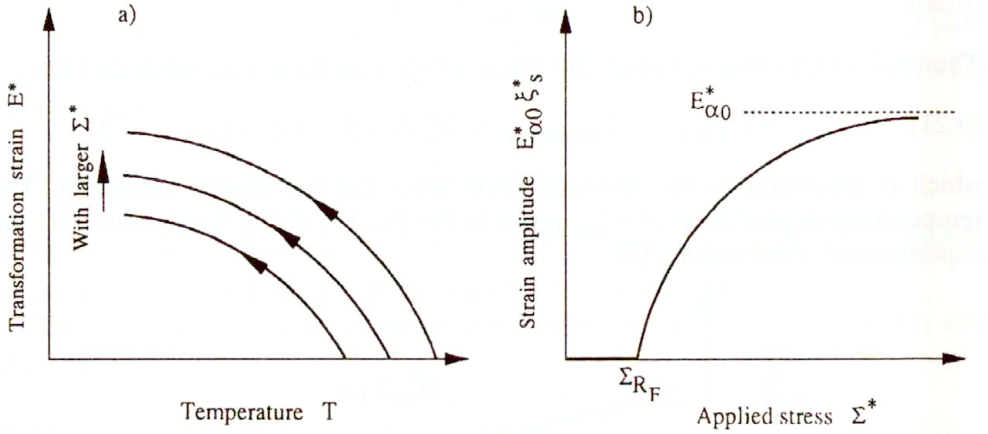

FIG. 5. Transformation strain during cooling (schematic).

Figure 5a shows a schematic plot of the transformation strain E^* vs. the temperature T with the applied stress Σ^* as a parameter. The curve shifts to the higher strain and higher temperature sides with the larger applied stress. The later shift stems simply from the positive slope of the R-phase transformation line, while the former shift comes from the stress-dependence of the amplitude $E^*_{\alpha 0}\zeta^*_s$ in Eq. (6.22). The amplitude gradually tends to a limit value with Σ^* as illustrated in Fig. 5b. So does the strain-temperature curve.

6.4. Cooling/heating under constant applied stress

Suppose the cooling stops at a lower limit temperature T_l and a heating process follows, always under a constant stress Σ^*. In order to take into account the hysteretic behaviour in α during the process, the reverse lattice distortion in the R-phase is assumed to be governed not by Eq. (6.1) but by

$$\dot{\alpha} = a_h(A_{T0} - \alpha)\dot{T}, \tag{6.25}$$

with a different material parameter a_h. Equation (6.25) is solved to give

$$\alpha = \alpha_l + (A_{T0} - \alpha_l)[1 - \exp a_h(T_l - T)] \tag{6.26}$$

with α_l, the value of α at T_l. Since the R-phase inverse transformation finishes at the thermomechanical load state $(T^*_{R_R}, \Sigma^*)$ on the R-phase reverse transformation line (cf. Fig. 3b) expressed by

$$\Sigma = c(T - T_{R_R}), \qquad T^*_{R_R} = T_{R_R} + \Sigma^*/c, \tag{6.27}$$

the parameter a_h introduced in Eq. (6.25) can be estimated from a set of the material parameters by

$$a_h = \frac{1}{T_l - T^*_{R_R}} \ln \frac{A_{T0}}{A_{T0} - \alpha_l}. \tag{6.28}$$

The macroscopic strain observed in the heating process is, by taking Eq. (6.14) into account, given by

$$E^* = E^*_{\alpha 0}\, \zeta^*_s \alpha + \int_{\alpha_l}^{\alpha} E^*_{\alpha 0}\, \zeta^*_s \, d\alpha + \int_{\zeta^*_s}^{\zeta} \Omega^*_\alpha \alpha \, d\zeta \,, \tag{6.29}$$

where the first term stands for the strain at the start of heating, cf. Eq. (6.22), while the second integral with respect to ζ works only at the temperature range between the R-phase transformation line and the R-phase reverse transformation line, i.e., between $T^*_{R_F}$ and $T^*_{R_R}$, in which the forward reorientation occurs.

The total macroscopic strain after a cycle of thermal loading under constant applied stress, $T^*_{R_F} \to T_l \to T^*_{R_R}$, is calculated to be

$$E^*_{\text{total}} = \Omega^*_\alpha \int_{T^*_{R_F}}^{T^*_{R_R}} \{\alpha_l + (A_{T0} - \alpha_l)[1 - \exp a_h(T_l - T)]\} \times (1 - \zeta^*_s)\overline{Z}_\Sigma b \exp\left[\overline{Z}_\Sigma b(T_l - T)\right] dT, \tag{6.30}$$

which is expected to be a small value since according to the experiments, the width of the R-phase transformation line and the R-phase reverse transformation line is narrow; $T^*_{R_R} - T^*_{R_F} \approx 5\,\text{K}$.

6.5. Thermomechanical process

Let us estimate the macroscopic strain developed during a thermomechanical loading sketched in Fig. 6 by the points 1 to 6, which is composed of the consecutive processes; cooling down to T_l under stress-free state ($1 \to 2$), isothermal loading up to Σ^* at T_l ($2 \to 3$), isostatic cooling down to T_l under Σ^* ($3 \to 4$) and isostatic heating up to $T^*_{R_R}$ under Σ^* ($4 \to 3 \to 5 \to 6$). The macroscopic strain induced in each of the processes is already calculated;

The cooling process ($1 \to 2$): No strain observed.

The isothermal loading up to Σ^* ($2 \to 3$): Eq. (6.20).

The process of cooling down to T_l ($3 \to 4$) under constant applied stress: Eq. (6.22).

The process of heating up to $T^*_{R_R}$ ($4 \to 3 \to 5 \to 6$) under constant applied stress: Eq. (6.30).

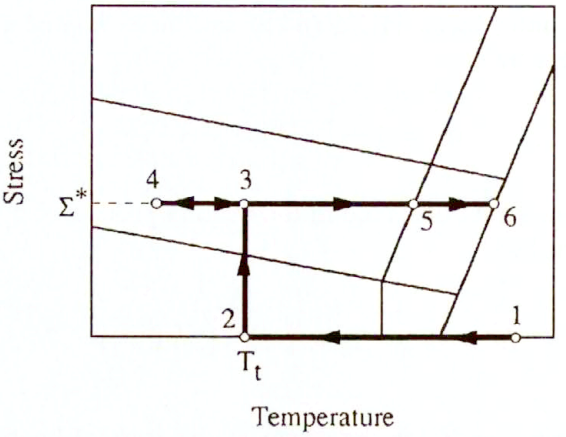

FIG. 6. Thermomechanical processes.

6.6. Recovery stress during heating

The simulation in the preceding subsections shows that a shrinkage strain is observed during heating along any kind of thermomechanical path. A tensile stress is, therefore, induced in the specimen when the strain is constrained during heating. The stress is called the recovery stress and plays an important role of the driving force in the shape memory devices. Change in stress under the condition of the constrained strain is incrementally governed by

$$0 = S\,d\Sigma + \Theta\,dT + dE^*, \tag{6.31}$$

which is derived from Eq. (6.15). The essential thing is, therefore, to calculate the increment of transformation strain dE^* along a prescribed thermomechanical loading path, which is already performed by means of Eq. (6.14) together with Eqs. (6.4) and (6.25). If the result is combined with Eq. (6.31), one obtains

$$\begin{aligned} d\Sigma = &- \left[S + \delta_\zeta \overline{Z}_\Sigma \Omega^*_\alpha \alpha(1-\zeta)\right]^{-1} \\ &\times \left[\Theta + \delta_\alpha E^*_{\alpha 0} \zeta^*_s a_h (A_{T0} - \alpha) + \delta_\zeta b\, \overline{Z}_\Sigma \Omega^*_\alpha \alpha(1-\zeta)\right] dT, \end{aligned} \tag{6.32}$$

which determines the stress increment $d\Sigma$ due to prescribed temperature increment dT. The indicators δ_ζ and δ_α have the following meaning:

$$\delta_\zeta = \begin{cases} 1 & \text{when the crystal reorientation progresses,} \\ 0 & \text{otherwise,} \end{cases}$$

$$\delta_\alpha = \begin{cases} 1 & \text{when the reverse lattice distortion in the R-phase progresses,} \\ 0 & \text{otherwise.} \end{cases}$$

From the practical point of view, the recovery stress induced during heating after the following two thermomechanical paths is important to be investigated: the process in which the residual strain is constrained at the point 2 in Fig. 6 after the successive thermomechanical preloading of the cooling ($1 \rightarrow 2$), loading ($2 \rightarrow 3$) and unloading ($3 \rightarrow 2$); and the process in which the total strain is constrained at the point 3 after the successive thermomechanical preloading of the cooling ($1 \rightarrow 2$) and loading ($2 \rightarrow 3$). The simulated results will be given in the next section.

7. Numerical illustrations

Uniaxial behaviours explained in Sec. 6 are simulated in this section with the use of the value of the material parameters tabulated in Table 1, which are partly determined from the data of a TiNi alloy [2], the transformation lines of which are illustrated in Fig. 7. The thermal strain is neglected in the following simulation.

Table 1. Material parameters.

S	a_c	b	c	$\overline{Z}_\Sigma$	T_{R_F}	T_{R_R}	Σ_{R_F}	A_{T0}	$\Omega^*_{\alpha_0}$	$E^*_{\alpha_0}$
1/MPa	1/K	MPa/K	MPa/K	1/MPa	K	K	MPa			
5×10^{-5}	−0.026	0.163	12	0.0132	300	310	10	1.2	0.01	0.01

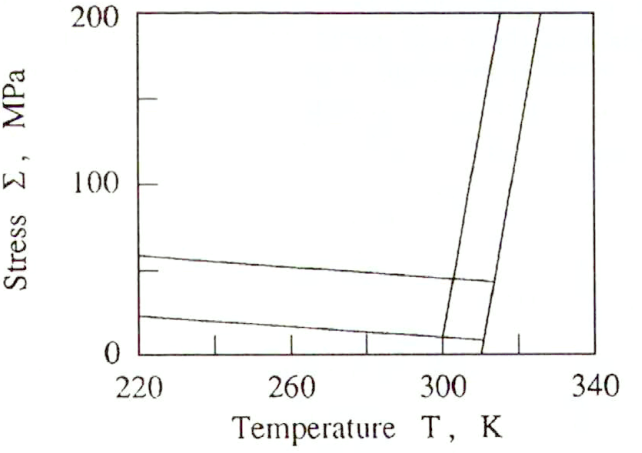

FIG. 7. Transformation lines.

Figure 8 shows the stress-strain curves observed during each isothermal loading and unloading at T_t in the successive cooling-loading-unloading processes ($1 \rightarrow 2 \rightarrow 3 \rightarrow 2$ in Fig. 6). It should be noted that the strain induced in this process is due only to the variants reorientation (cf. Sec. 6.2). The ferroelastic curves exhibit, under the temperature range of $T_t \leq T_{R_F} = 300\,\mathrm{K}$, the same response as

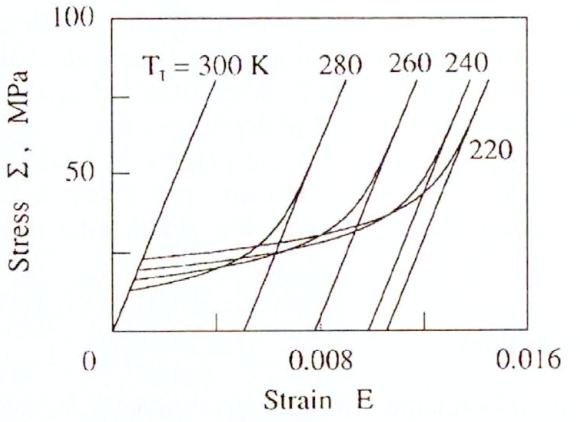

FIG. 8. Stress-strain curves.

the shape memory effect in the martensitic transformation. The strain amplitude, the recovery strain E^*_{max}, at each temperature is plotted in Fig. 9, which corresponds to the schematic illustration in Fig. 4 and represents well the experimental observation [2]. Figure 10 is a plot of the transformation strain E^* observed when the applied stress at the state 3 in Fig. 6 is Σ^*. The results show firstly that, for the higher stress and higher temperature, the transformation strain converges at the earlier stage to a limit curve which corresponds to the curve in Fig. 9. It is a rephrase of the fact that the variants reorientation finishes when the generic point reaches the variants reorientation finish line in Fig. 3 c, d. Secondly, the lower intersection of the iso-Σ^* curve with the horizontal line represents the point on the variants reorientation start line in Fig. 3 c, d at which the variants reorientation starts and the transformation strain starts being induced.

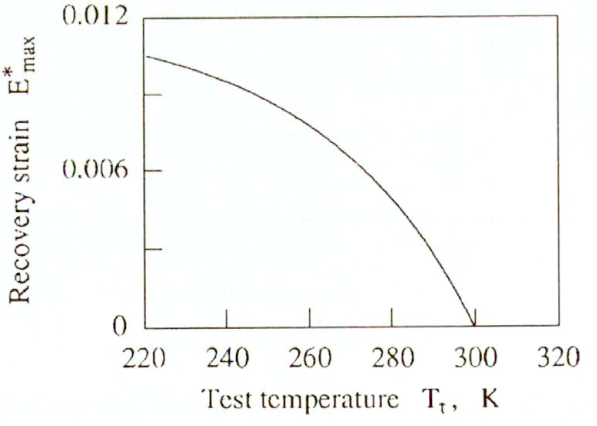

FIG. 9. Temperature dependence of recovery strain.

Figure 11 illustrates the development of the transformation strain E^* in the isostatic cooling processes ($6 \rightarrow 5 \rightarrow 3 \rightarrow 4$ in Fig. 6) down to $T_l = 220\,\mathrm{K}$ under

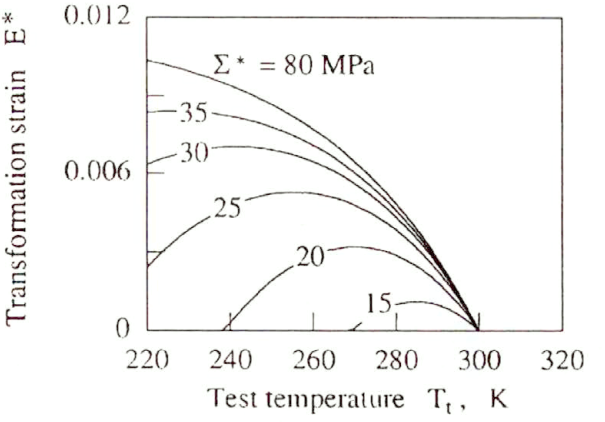

FIG. 10. Stress and temperature dependence of recovery strain.

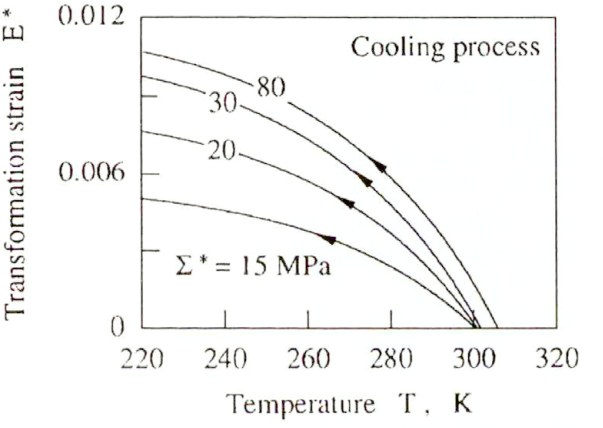

FIG. 11. Change in transformation strain during cooling under constant applied stress.

a constant applied stress Σ^*. As explained in Sec. 6.3, the strain is induced only by the forward lattice distortion in the R-phase. Two points have to be noted: the transformation strain increases with Σ^* and converges to a limit curve at each temperature level. Secondly, the temperature of the strain to start being induced increases with the applied stress, which is due to nothing other than the fact that the R-phase transformation line has a positive inclination as shown in Fig. 3 a.

Under the cooling/heating processes ($6 \rightarrow 5 \rightarrow 3 \rightarrow 4 \rightarrow 3 \rightarrow 5 \rightarrow 6$ in Fig. 6) down to $T_l = 220\,\mathrm{K}$ under a constant applied stress Σ^*, the strain induced in the cooling process, which has already been calculated above, fully recovers in the subsequent heating process as given in Fig. 12. The strain vanishes on the R-phase reverse transformation line (cf. Fig. 3 b), meaning at different temperatures. The change in transformation strain stems from the reverse lattice distortion process in the R-phase. The variants reorientation progresses in the heating process only

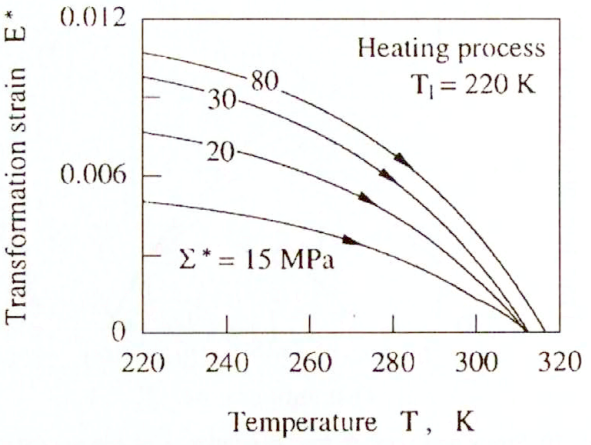

FIG. 12. Change in transformation strain during heating under constant applied stress.

in a narrow region between the R-phase transformation line and the R-phase reverse transformation line, which has no notable effect on the results. The change in transformation strain during the whole cooling/heating process is plotted in Fig. 13 in the case of T_l = 220 K under Σ^* = 20 MPa. The transformation strain increases in the cooling process and recovers fully in the subsequent heating process. A hysteresis is observed due to the fact that the R-phase transformation line and the R-phase reverse transformation line are different.

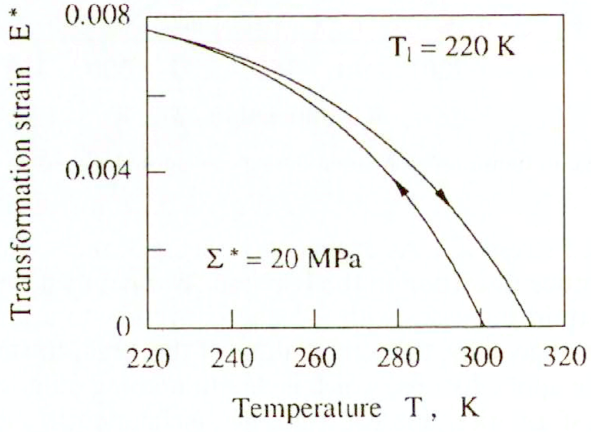

FIG. 13. Strain hysteresis during cooling/heating under constant applied stress.

When the specimen is heated after a cooling-loading-unloading process ($1 \rightarrow 2 \rightarrow 3 \rightarrow 2$ in Fig. 6), with the residual strain at the state 2 constrained, a positive recovery stress is induced, which is plotted in Fig. 14 for the cases of the isothermal loading to Σ^* at T_t = 220 K. The variants reorientation progresses up to an extent ζ^* when Σ^* is in the variants reorientation zone in Fig. 3 c dur-

ing isothermal loading. During heating, a negative increase of the transformation strain first progresses due to the reverse lattice distortion in the R-phase. A positive increase of the recovery stress is, therefore, observed at this stage as shown in the figure. When the generic point (T, Σ_R) reaches the ζ^* line, the variants reorientation starts progressing from the extent ζ^* on. The process induces a positive strain increase, resulting in a decrease of the stress. From this moment on, two metallurgical progresses occur simultaneously. The reverse lattice distortion in the R-phase increases the recovery stress, whereas the variatns reorientation decreases the recovery stress. The case is typically observed in the figure for the cases of Σ^* = 25, 30 and 35 MPa. When Σ^* is large, the variants reorientation almost finishes during the first isothermal loading. No decrease in recovery stress is, therefore, observed in the subsequent heating process (cf. the case of Σ^* = 80 MPa). When Σ^* is lower than the variants reorientation start line, neither the residual strain nor the recovery stress is produced.

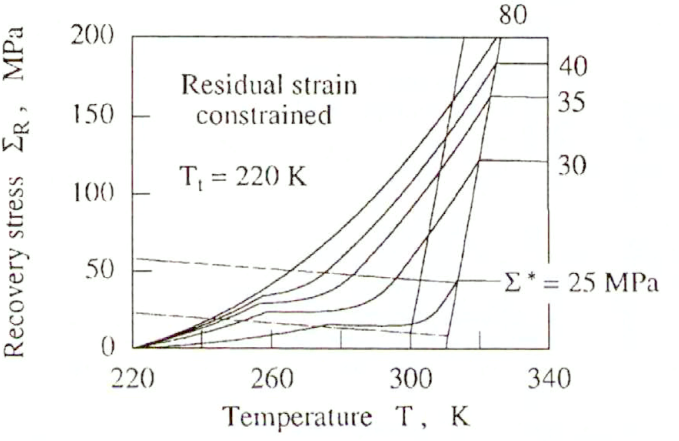

FIG. 14. Recovery stress under residual strain constrained.

The maximum recovery stress $\Sigma_{R\,\max}$ is reached on the R-phase reverse transformation line, which is plotted in Fig. 15 versus the test temperature T_t with the applied stress Σ^* as a parameter. The intersections of the iso-Σ^* curves and the horizontal axis are on the variants reorientation start line.

When the specimen is heated after a cooling-loading process ($1 \rightarrow 2 \rightarrow 3$ in Fig. 6), with the total strain constrained at the state 3 (T_t, Σ^*), the recovery stress starts increasing from the initial value Σ^* as given in Fig. 16. The two metallurgical processes occur simultaneously when the start point is in the variants reorientation zone, as in the case of the constrained residual strain (Fig. 14). The variants reorientation process finishes when the generic point reaches the finish line on each iso-Σ^* curve. The remaining process progresses only due to the reverse lattice distortion in the R-phase. A slower increase in the strain for the lower value of Σ^* is a point to be noted when comparing the simulated results with the experimental data.

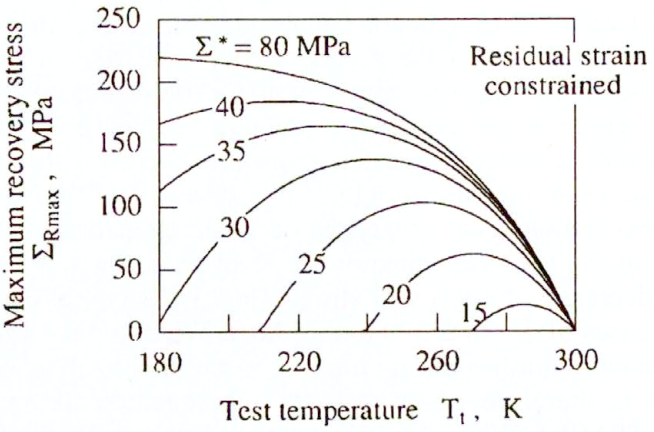

FIG. 15. Maximum recovery stress under residual strain constrained.

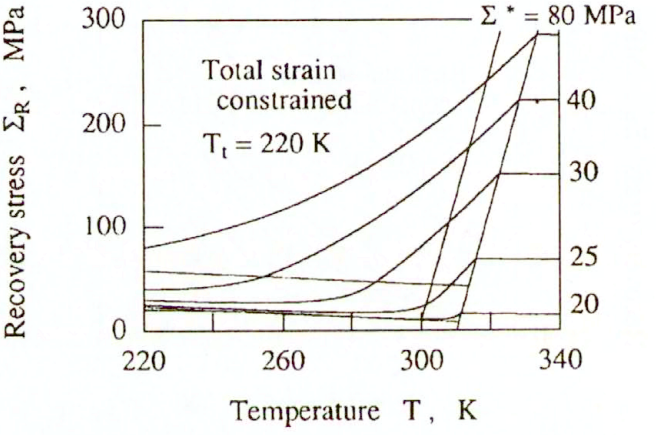

FIG. 16. Recovery stress under total strain constrained.

8. Concluding remarks

The metallurgical observations have clearly revealed in the TiNi shape memory alloys that the R-phase transformation starts on a R-phase transformation start line in the stress-temperature plane and finishes on the other line, the R-phase transformation finish line. The same is true for the R-phase reverse transformation being represented by the R-phase reverse transformation start/finish lines. The processes which have mistakenly been understood as the R-phase transformation in the mechanical formulations carried out so far, include the processes "after" the R-phase transformation, the lattice distortion in the R-phase variants and the variants reorientation of the R-phase variants by twinning.

The theoretical framework established in this paper on the thermomechanics of R-phase transformation is based on this metallurgical understanding. The

uniaxial governing equations are reduced from the general formulation in order to simulate the alloy behaviour under several thermomechanical load processes. The validity of the theory can be well proved by carrying out the experiments on the recovery stress explained in Figs. 14 and 15, which show a clear coupled effect of the lattice distortion in the R-phase and the variants reorientation. This is a task of the next study.

Acknowledgments

Part of this work was financially supported by the Special Research Fund/Tokyo Metropolitan Government as well as by the Grant-in-Aid for Scientific Research (No. 08611507) through the Ministry of Education, Science and Culture, Japan.

References

1. S. MIYAZAKI and K. OTSUKA, *Deformation and transition behavior associated with the R-phase in Ti-Ni alloys*, Metall. Trans. A, **17A**, 53–63, 1986.
2. S. MIYAZAKI and C.M. WAYMAN, *The R-phase transition and associated shape memory mechanism in TiNi single crystals*, Acta Metall., **36**, 181–192, 1988.
3. S. MIYAZAKI, S. KIMURA and K. OTSUKA, *Shape-memory effect and pseudoelasticity associated with the R-phase transition in Ti-50.5 at. % Ni single crystals*, Phil. Mag. A, **57**, 467–478, 1988.
4. S. MIYAZAKI, K. NOMURA and A. ISHIDA, *Shape memory effects associated with the martensitic and R-phase transformations in sputter-deposited Ti-Ni thin films*, J. Physique IV, Coll. C8, suppl. J. Phys. III, vol. 5, C8/677-C8/682, 1995.
5. T. SAWADA, H. TOBUSHI, K. KIMURA, T. HATTORI, K. TANAKA and P.H. LIN, *Stress-strain-temperature relationship associated with the R-phase transformation in TiNi shape memory alloy (Influence of shape memory processing temperature)*, JSME Int. J., Ser. A, **36**, 395–401, 1993.
6. P.H. LIN, H. TOBUSHI, Y. HATTORI, K. TANAKA and CH. LEXCELLENT, *Recovery stress associated with the R-phase transformation in TiNi shape memory alloy*, [in:] Proc. First ASIA-Oceania Int. Symp. on Plasticity, WANG TZUCHIANG and XU BINGYE [Eds.], Peking University Press, Beijing, 72–79, 1994.
7. P.H. LIN, H. TOBUSHI, A. IKAI and K. TANAKA, *Deformation properties associated with the martensitic and R-phase transformations in TiNi shape memory alloy*, [in:] Shape Memory Materials 94, CHU YOUYI and TU HAILING [Eds.], International Academic Publishers, 530–534, 1994.
8. S. LECLERCQ, CH. LEXCELLENT, H. TOBUSHI and P.H. LIN, *Thermodynamical modelling of recovery stress associated with R-phase transformation in TiNi shape memory alloys*, Mater. Trans., JIM, **35**, 325–331, 1994.
9. C.M. HWANG, M.E. MEICHLE, M.B. SALAMON and C.M. WAYMAN, *Transformation behavior of a $Ti_{50}Ni_{47}Fe_3$ alloy*, II. *Subsequent premartensitic behavior and the commensurate phase*, Phil. Mag. A, **47**, 31–62, 1983.
10. M.B. SALAMON, M.E. MEICHLE and C.M. WAYMAN, *Premartensitic phases of $Ti_{50}Ni_{47}Fe_3$*, Phys. Rev., **B31**, 7306–7315, 1985.
11. H.C. LING and R. KAPLOW, *Phase transitions and shape memory in NiTi*, Metall. Trans. A, **11A**, 77–83, 1980.
12. H.C. LING and R. KAPLOW, *Stress-induced shape changes and shape memory in the R and martensite transformations in equiatomic NiTi*, Metall. Trans. A, **12A**, 2101–2111, 1981.
13. H.B. CALLEN, *Thermodynamics*, John Wiley & Sons, New York 1960.
14. D.J. BARRETT, *A three-dimensional phase transformation model for shape memory alloys*, J. Intell. Material Syst. Struct., **6**, 831–840, 1995.

15. L.C. BRINSON, A. BEKKER and S. HWANG, *Deformation of shape memory alloys due to thermo-induced transformation*, J. Intell. Material Syst. Struct., 7, 97–107, 1996.

16. L.C. BRINSON, *One-dimensional constitutive behavior of shape memory alloys: Thermomechanical derivation with non-constant material functions and redefined martensite internal variable*, J. Intell. Material Syst. Struct., **4**, 229–242, 1993.

17. Q.P. SUN and K.C. HWANG, *Micromechanics modelling for the constitutive behavior of polycrystalline shape memory alloys. I. Derivation of general relations*, J. Mech. Phys. Solids, **41**, 1–17, 1993.

18. E. PATOOR, A. EBERHARDT and M. BERVEILLER, *Micromechanical modelling of the shape memory behavior*, [in:] Mechanics of Phase Transformations and Shape Memory Alloys, L.C. BRINSON and B. MORAN [Eds.], ASME, New York, 23–37, 1994.

19. S. LECLERCQ, CH. LEXCELLENT, *A general macroscopic description of the thermomechanical behavior of shape memory alloys*, J. Mech. Phys. Solids, **44**, 953–980, 1996.

20. K. TANAKA, S. KOBAYASHI and Y. SATO, *Thermomechanics of transformation pseudoelasticity and shape memory effect in alloys*, Int. J. Plasticity, **2**, 59–72, 1986.

21. K. TANAKA, E.R. OBERAIGNER and F.D. FISCHER, *A unified theory on thermomechanical mesoscopic behavior of alloy materials in the process of martensitic transformation*, [in:] Mechanics of Phase Transformations and Shape Memory Alloys, L.C. BRINSON and B. MORAN [Eds.], ASME, New York, 151–157, 1994.

22. B. RANIECKI and A. SAWCZUK, *Thermal effect in plasticity. Part I. Coupled theory*, ZAMM, **55**, 333–341, 1975.

23. K. TANAKA, F. NISHIMURA, H. TOBUSHI, E.R. OBERAIGNER and F.D. FISCHER, *Thermomechanical behavior of an Fe-based shape memory alloy: Transformation conditions and hystereses*, [in:] Proc. ICOMAT 95, J. Physique IV, Coll. C8, Suppl. J. Phys. III, Vol. 5, R. GOTTHARDT and J. VAN HUMBEECK [Eds.], Les Editions De Physique, Les Ulis, C8/463-C8/468, 1995.

24. F. NISHIMURA, N. WATANABE and K. TANAKA, *Transformation lines in an Fe-based shape memory alloy under tensile and compressive stress states*, Materials Sci. Engng. A, **221**, 134–142, 1996.

25. D.G.B. EDELEN, *Primitive thermodynamics: A new look at the Clausius-Duhem inequality*, Int. J. Engng. Sci., **12**, 121–141, 1974.

26. A.C. ERINGEN, *Thermodynamics of continua*, [in:] Continuum Physics, A.C. ERINGEN [Ed.], Vol. II, Part I-3, Academic Press, New York, 89–127, 1975.

27. D. PERIC, *On a class of constitutive equations in viscoplasticity: formulation and computational issues*, Int. J. Num. Methods Engng., **36**, 1365–1393, 1993.

DEPARTMENT OF AEROSPACE ENGINEERING,
TOKYO METROPOLITAN INSTITUTE OF TECHNOLOGY, HINO/TOKYO
e-mail: kikitana@astan1.tmit.ac.jp

and

INSTITUTE OF MATERIALS SCIENCE
UNIVERSITY OF TSUKUBA, TSUKUBA, J-305 IBARAKI, JAPAN

Received April 17, 1996; new version December 12, 1996.